Northumbria Research Link

Northumbria University
NEWCASTLE

UniversityLibrary

Spectrally-isolated violet to blue wavelength generation by cascaded degenerate four-wave mixing in a photonic crystal fiber

Jinhui Yuan[1,2,†,*], Zhe Kang[2,†], Feng Li[2], Xianting Zhang[2], Guiyao Zhou[3], Xinzhu Sang[1,*], Qiang Wu[4], Binbin Yan[1], Xian Zhou[2], Liang Wang[2], Kangping Zhong[2], Kuiru Wang[1], Chongxiu Yu[1], Hwa Yaw Tam[2], and P. K. A. Wai[2]

[1]*State Key Laboratory of Information Photonics and Optical Communications (Beijing University of Posts and Telecommunications), P.O. Box163 (BUPT), 100876 Beijing, China*
[2]*Photonics Research Centre, Department of Electronic and Information Engineering, The Hong Kong Polytechnic University, Hong Kong*
[3]*Guangdong Provincial Key Laboratory of Nanophotonic Functional Materials and Devices, South China Normal University, 510006 Guangzhou, China*
[4]*Department of Physics and Electrical Engineering, Northumbria University, Newcastle upon Tyne, NE1 8ST, United Kingdom*
†These authors contributed equally to this work.
*Corresponding authors: yuanjinhui81@163.com *and xzsang@bupt.edu.cn*

Generation of spectrally-isolated wavelengths in the violet to blue region based on cascaded degenerate four-wave mixing (FWM) is experimentally demonstrated for the first time in a tailor-made photonic crystal fiber (PCF), which has two adjacent zero dispersion wavelengths (ZDWs) at 696 and 852 nm in the fundamental mode. The influences of the wavelength λ_p and the input average power P_{av} of the femtosecond pump pulses on the phase-matched frequency conversion process are studied. When femtosecond pump pulses at λ_p of 880, 870, and 860 nm and P_{av} of 500 mW are coupled into the normal dispersion region close to the second ZDW, the first anti-Stokes waves generated near the first ZDW act as a secondary pump for the next FWM process. The conversion efficiency η_{as2} of the second anti-Stokes waves, which are generated at the violet to blue wavelengths of 430, 456, and 472 nm, are 4.8, 6.48, and 9.66%, for λ_p equals 880, 870, and 860 nm, respectively.

Generation of discrete new wavelengths in the violet to blue spectral region has important applications in basic physics and applied science. The control in fiber dispersion and nonlinearity properties available in the fabrication process of photonic crystal fibers (PCFs) [1] enables supercontinuum (SC) generation [2-5] or a particular nonlinear effect in PCFs to be used to convert the energy of available laser output to new spectral regions of interest. Spectrally-isolated blue and violet wavelengths can be obtained through selective filtering the SC, but the temporal width of the filtered wavelengths would be broadened and the output power lowered. The dispersive waves generated by soliton dynamics [6-8] in the rare-earth-doped solid-core PCFs [9] or gas-filled hollow-core PCFs [10] can be used to extend the near-infrared femtosecond laser output at 800 nm to the blue and violet or even shorter wavelengths, but a complex laser system is needed to provide the milli-joule, sub-100 fs laser output required. The optical properties of the rare-earth ions and gases of the PCFs have to be considered also.

Four-wave mixing (FWM) is one of the nonlinear parametric processes that can be used to generate new optical wavelengths. In order to directly generate discrete violet to blue wavelengths by phase-matched FWM [11-14], the pump wavelengths should be located in the normal dispersion region close to the zero dispersion wavelengths (ZDWs) below 700 nm in the fundamental mode of a PCF, the relative air-hole sizes of which should be greater than 0.8 and the core diameters less than 1.5 μm. However, the laser sources to achieve the phase-matched condition are not currently available. Such PCFs are also difficult to fabricate and suffer from high propagation loss and low damage threshold at the required incident power. Cascaded FWM, which occurs easily in common PCFs, does not face the same challenges in generating discrete violet to blue wavelengths. In cascaded FWM, the signal (anti-Stokes) and idler (Stokes) waves derived from the initial FWM serve as the pump wave for the next FWM process to generate new optical waves. Recently, broadband cascaded non-degenerate and degenerate FWM spectral components centered at the wavelengths of 1, 1.55, and 2 μm in PCFs have been demonstrated for frequency comb or SC generation when continuous waves or short pulses are used as the pump sources [15-21].

In this letter, a silica PCF with two adjacent ZDWs in the fundamental mode is fabricated in our laboratory. The cascaded degenerate FWM effect is studied when femtosecond pump pulses are launched into the normal dispersion region close to the second ZDW of 852 nm in the fundamental mode of the PCF. The first anti-Stokes waves are generated near the first ZDW of 696 nm, and then it is used as the pump for the next FWM process. By the cascaded degenerate FWM effect, for the first time spectrally-isolated second anti-Stokes waves are generated within the violet to blue wavelength range from 430 to 472 nm.

Fig. 1(a) shows a tailor-made silica PCF with hexagonal lattice geometry in the cladding region. The core diameter is 1.63 μm, and average relative air-hole diameter is 0.65. Fig. 1(b) shows the calculated group-velocity dispersion curve of the fundamental mode of the PCF, where the two ZDWs are located at 696 and 852 nm, respectively. From Fig. 1(b), the anomalous dispersion region between the two ZDWs covers a wavelength range of 156 nm with a dispersion value less than 12 ps/nm/km. The nonlinear coefficient around 850 nm, estimated from the effective mode area, is 0.117 $W^{-1}m^{-1}$. When the initial pump pulses are coupled to the normal dispersion region close to the second ZDW, the energy from the incident pump is converted to the spectrally-isolated anti-Stokes waves at the shorter wavelengths by

degenerate FWM because the narrow anomalous dispersion region and the low dispersion value reduce the group-velocity mismatches between all the optical waves involved. The inset of Fig. 1(b) shows the fundamental spatial mode profile calculated at wavelength of 850 nm, which takes on the characteristic of the Gaussian distribution.
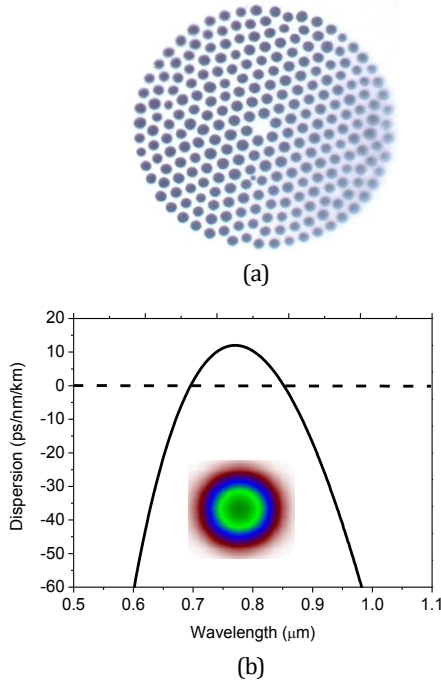

(a)

(b)

Fig. 1. (a) The cross-sectional structure of the PCF used, and (b) the group-velocity dispersion curve of the fundamental mode. The inset shows the fundamental spatial mode profile calculated at 850 nm.

In the experiment, we use a set-up similar to that used in our previous work [22]. The pump pulses are provided by a mode-locked Ti:sapphire laser, which operates at the tunable wavelength range of 780 to 900 nm and emits 120 fs pulse trains at a repetition rate of 76 MHz. The incident pump light passes through an optical isolator to suppress any optical reflection, and is coupled by a 40× microscope objective into the fundamental mode of a span of PCF with a length of 36 cm. The coupling state of the pump light is monitored by a CCD camera. The free-space coupling efficiency is about 58%, and the input pump powers can be adjusted by a variable optical attenuator. The output spectra from the PCF are recorded by an optical spectrum analyzer (OSA, Avaspec-256) with a wavelength range of 200 to 1100 nm, and the output powers of the optical waves of interest can be measured by a combination of the optical filters at different wavelengths and an optical power meter.

In degenerate FWM, the anti-Stokes waves at the up-shifted optical frequency ω_{as} and Stokes waves at the down-shifted optical frequency ω_s are generated from the incident pump wave at the initial optical frequency of ω_p when energy and momentum conservations are satisfied at the same time. The phase-matched condition derived from momentum conservation depends on the material of the PCF, geometry of the waveguide structure, and nonlinearity, as described in Ref [22]. Fig. 2(a) shows the calculated phase-mismatched parameter κ when the initial pump pulses with wavelength λ_p of 880 nm and average input power P_{av} of 500 mW (the corresponding peak power equals to 60 kW) are launched into the normal dispersion region close to the second ZDW of 852 nm in the fundamental mode. From Fig. 2(a), κ equals zero at wavelength 725.4 nm, where the first anti-Stokes wave can be efficiently generated. Moreover, because the anti-Stokes wave generated at 725.4 nm is located near the first ZDW of 696 nm, it could serve as a pump for the next FWM process, and the second anti-Stokes wave may be generated at the shorter wavelength. Fig. 2(b) shows that the κ calculated without considering the nonlinearity contribution reaches zero at the blue wavelength of 472.3 nm for the secondary

pump wavelength at 725.4 nm. The contribution of nonlinearity to κ is negligible because the peak power of the first anti-Stokes wave, which is used as the secondary pump, is greatly reduced. It is a consequence of the rapid broadening of the anti-Stokes pulse induced by the dispersive and nonlinear effects.
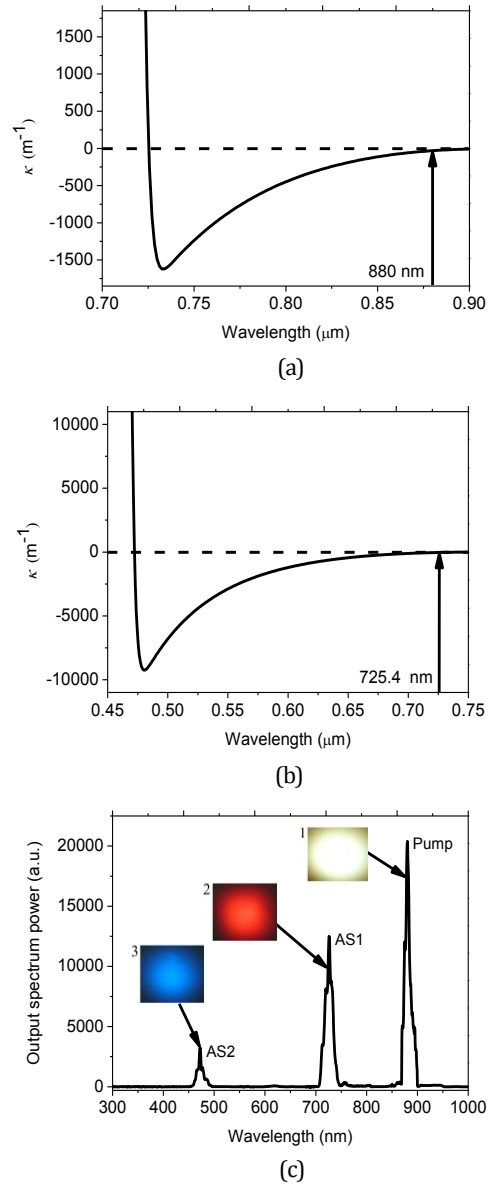

(a)

(b)

(c)

Fig. 2. The phase-mismatched parameters κ calculated for the fundamental mode of the PCF (a) in the first FWM process with the nonlinearity contribution considered at the input pump pulses wavelength λ_p at 880 nm and (b) in the second FWM process without considering the nonlinearity contribution. The input average power P_{av} is 500 mW (corresponding peak power 60 kW). (c) The observed output spectrum from the PCF under the same pump condition. Insets 1, 2, and 3 show the output far fields at the pump and anti-Stokes wavelengths of 880, 726, and 472 nm, with the white, red, and blue light, respectively.

Fig. 2(c) shows the output spectrum from the 36 cm-long PCF recorded by the OSA under the same pump condition. Initially, the self-phase modulation (SPM), self-steepening, and Raman effects lead to asymmetrical broadening of the incident spectrum of the pump wave. The spectrally-isolated first and second anti-Stokes waves are generated at the visible wavelengths of 726 and 472 nm through cascaded degenerate FWM, and the pump power is greatly depleted. The experimental result agrees well with the theoretical one. We note that although the first anti-Stokes wave is located in the anomalous

dispersion region, soliton dynamics do not occur. It is the result of the very narrow anomalous dispersion region (156 nm) and low dispersion value (less than 12 ps/nm/km) of the PCF used. The soliton can not be formed here [23, 24]. Most of the generated first anti-Stokes wave power will be transferred out of the anomalous dispersion region by the combined SPM and second FWM processes. In addition, it is expected that Stokes waves would be generated at the near-infrared wavelengths of 1117 and 1572 nm, which correspond to the same frequency shift as the anti-Stokes waves, but they fall outside the range of the OSA and are beyond our consideration. Insets 1, 2, and 3 of Fig. 2(c) respectively show the Gaussian-like far field mode patterns at the pump, first, and second anti-Stokes wavelengths observed from the output end of the PCF, which are consistent with that shown in the inset of Fig. 1(b).

Fig. 3(a) shows the κ calculated for the first degenerated FWM with the nonlinear contribution at pump pulse wavelength λ_p = 860 nm. At P_{av}=300, 400, and 500 mW (peak powers equal to 36, 48, and 60 kW), κ=0 is satisfied at the visible wavelengths of 715.7, 704.4, and 689.1 nm, respectively. Similarly, Fig. 3(b) shows κ calculated for the second degenerated FWM without the nonlinear contribution. The wavelengths for κ=0 are 457.9, 447.3, and 429.5 nm, at P_{av}=300, 400, and 500 mW, respectively. The first and second anti-Stokes waves could be generated at these wavelengths. Fig. 3(c) shows the experimental spectra observed from the output end of the PCF. From Fig. 3(c), the first anti-Stokes waves are centered at the wavelengths of 716, 705, and 689 nm, and the second anti-Stokes waves are centered at 458, 447, and 430 nm, for input average power 300, 400, and 500 mW, respectively. The experimental results agree well with the calculation results shown in Fig. 3(a) and 3(b). The inset of Fig. 3(d) shows that the first and second anti-Stokes wavelengths λ_{as1} and λ_{as2} depends almost linearly with P_{av}. Fig. 3(d) shows the dependences of the measured output power P_{as2} of the second anti-Stokes waves and the conversion efficiency η_{as2}, which is defined as the power ratio of the generated second anti-Stokes waves and the incident pump, on P_{av}. Taking the coupling efficiency of 58% into account, P_{as2} is measured to be 3.76, 10.72, and 28.01 mW, and the corresponding η_{as2} are 2.16, 4.62, and 9.66%, at P_{av} = 300, 400, and 500 mW, respectively.
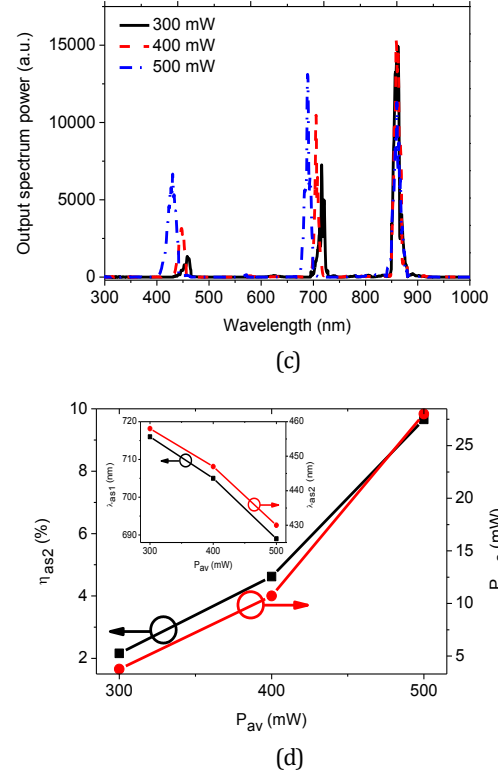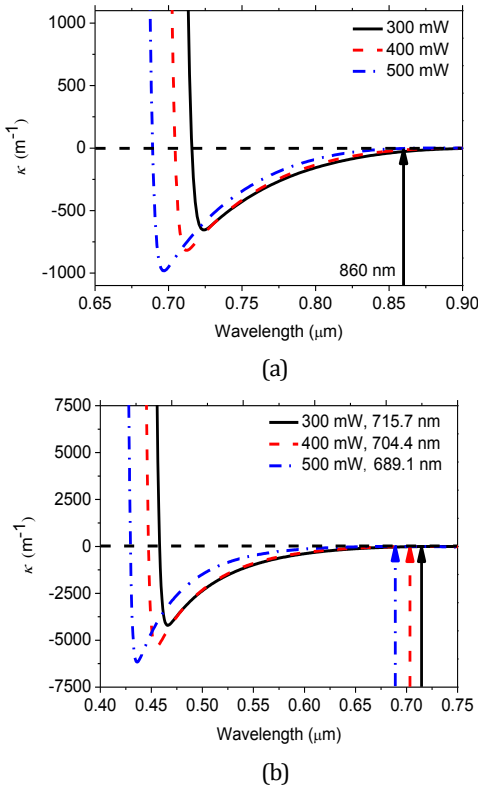
(c)

(d)

Fig. 3. The phase-mismatched parameters κ calculated for the fundamental mode of the PCF in the (a) first FWM process with the nonlinear contribution, and in the (b) second FWM process without the nonlinear contribution. The pump pulses are at 860 nm. The input average power P_{av}=300, 400, and 500 mW (corresponding peak powers of 36, 48, and 60 kW). (c) The observed output spectra under the same pump condition. (d) The dependences of the measured corresponding conversion efficiency η_{as2} (black solid-square line) and output power P_{as2} (red solid-circular line) of the second anti-Stokes waves on P_{av}. The inset shows the relationships between the first (λ_{as1}) (black solid-square line) and second (λ_{as2}) (red solid-circular line) anti-Stokes wavelengths and P_{av}.

By comparing Fig. 2(c) and Fig. 3(c), for λ_p =880 and 860 nm and P_{av}= 500 mW, we observed that the powers of the generated second anti-Stokes wave are evidently raised when the first anti-Stokes waves, which are used as a secondary pump for the next FWM process, are moved from 726 to 689 nm. The enhanced FWM-based energy conversion process is mainly due to the decrease in the interval between the center wavelengths of the first anti-Stokes wave and the second ZDW (696 nm) of the PCF used [25]. Finally, Fig. 4(a) shows that when the pump pulses at P_{av} = 500 mW and λ_p = 880, 870, and 860 nm, respectively, are propagated inside the PCF, the second anti-Stokes waves are generated at 472, 456, and 430 nm, respectively. The inset of Fig. 4(b) shows that λ_{as2} is tunable from 472 to 430 nm as λ_p shifts toward the second ZDW from 880, to 870, and to 860 nm. In the experiment, the single-mode propagation is well controlled, and the effective spatial overlaps between the initial pump wave, first, and second anti-Stokes waves are kept to achieve efficient power conversion. In Fig. 4(b), P_{as2} is measured to be 13.92, 18.79, and 28.01 mW at λ_p=880, 870, and 860 nm, respectively, and the corresponding η_{as2} are 4.8, 6.48, and 9.66%, respectively. The calculated η_{as2} for the initial pump pulses at λ_p = 860 nm and P_{av} = 500 mW is 12.4% assuming pump depletion, constant nonlinear coefficient, and no loss. The reasons for the discrepancy between the theoretical and experimental results are considered as follows. First, the propagation loss including the intrinsic absorption loss of the silica material, leaky loss, and scattering loss, reduces the output power of the anti-Stokes wave. Second, the variation of the PCF structure parameters along the longitudinal direction has a detrimental effect on the phase-matched-

(a)

(b)

dependent FWM process. Third, the group-velocity mismatch can separate the pump and anti-Stokes pulses involved after a short interaction length, which limits the efficiency of FWM. In future work, we will improve the fabrication technique and optimize the parameters of the PCF geometric structure in order to reduce the propagation loss and achieve good longitudinal uniformity of the PCF. In addition, we will choose the pump pulse parameters appropriately and use the seeded FWM process to alleviate the limitation imposed by the group-velocity mismatch [26].
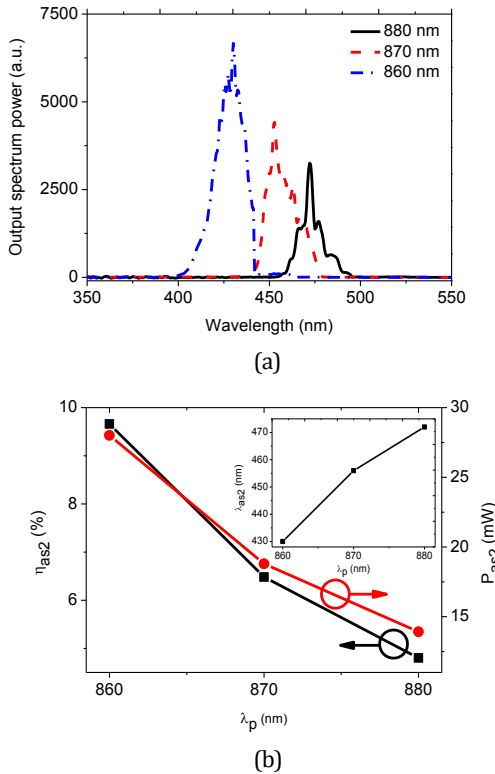

(a)

(b)

Fig. 4. (a) The observed output spectra at pump wavelength λ_p=880, 870, and 860 nm and input average power P_{av}= 500 mW (peak power of 60 kW). (b) The dependences of the measured conversion efficiency η_{as2} (black solid-square line) of the second anti-Stokes waves and the corresponding output power P_{as2} (red solid-circular line) on λ_p. The inset shows the relationship between the second anti-Stokes wavelength λ_{as2} (black solid-square line) and λ_p.

As shown in Fig. 4(a), the output spectra of the second anti-Stokes waves exhibit multiple peaks. The main reason is that part of the pump power is coupled into the other polarization state of the fundamental mode because of the small birefringence of the PCF, which could be the result of the slight irregularities in the core shape and cladding structure of the PCF. Also, the longitudinal non-uniformity of the PCF can lead to fluctuations of the dispersion of the fundamental mode and phase-matched profiles, which can have influences on the FWM process and the output spectrum impurity. Another possible reason is that the second anti-Stokes waves generated are converted to other higher-order guided-modes, which have different dispersion, polarization, and phase-matched properties. The nonlinear interactions involving different guided-modes show complex vectorial characteristic [27]. In addition, the SPM and Raman effects in the normal dispersion region could also affect the spectrum shapes and induce fine structures on the second anti-Stokes waves.

By appropriately designing the PCF geometric structure and selecting the pump pulse parameters, λ_{as2} can be widely tunable from the ultraviolet to visible spectral region. Moreover, we believe that this cascaded degenerate FWM process can be combined with other nonlinear optical techniques such as second-harmonic and sum-frequency generations to generate deep ultraviolet wavelengths.

In summary, by launching femtosecond pump pulses into the normal dispersion region close to the second ZDW in the fundamental mode of a tailor-made PCF with two adjacent ZDWs, we experimentally generate spectrally-isolated violet to blue wavelengths within the range of 430 to 472 nm by the cascaded degenerate FWM process. The tunable violet to blue wavelengths generated can find important applications in basic physics and applied science such as the study of multi-photon ionization, high-resolution optical imaging, etc.

References

[1] P. St. J. Russell, J. Lightw. Technol. **24**, 4729 (2006).
[2] J. M. Dudley, G. Genty, and S. Coen, Rev. Mod. Phys. **78**, 1135 (2006).
[3] A. A. Cumberland, J. C. Travers, S. V. Popov, and J. R. Taylor, Opt. Lett. **33**, 2122 (2008).
[4] J. M. Dudley, and J. R. Taylor, Nat. Photon. **3**, 85 (2009).
[5] S. P. Stark, J. C. Travers, and P. St. J. Russell, Opt. Lett. **37**, 770 (2012).
[6] I. Cristiani, R. Tediosi, L. Tartara, and V. Degiorgio, Opt. Express **12**, 124 (2004).
[7] H. H. Tu, and S. A. Boppart, Opt. Express **17**, 9858 (2009).
[8] G. Q. Chang, L. J. Chen, and F. X. Kärtner, Opt. Lett. **35**, 2361 (2010).
[9] G. P. Agrawal, *Applications of Nonlinear Fiber Optics* (Academic, 2008).
[10] N.Y. Joly, J. Nold, W. Chang, P. Hölzer, A. Nazarkin, G. K. L. Wong, F. Biancalana, and P. St. J. Russell, Phys. Rev. Lett. **106**, 203901-1 (2011).
[11] S. Asimakis, P. Petropoulos, F. Poletti, J. Y. Y. Leong, R. C. Moore, K. E. Frampton, X. Feng, W. H. Loh, and D. J. Richardson, Opt. Express **15**, 596 (2007).
[12] D. Nodop, C. Jauregui, D. Schimpf, J. Limpert, and A. Tünnermann, Opt. Lett. **34**, 3499 (2009).
[13] L. Lavoute, J. C. Knight, P. Dupriez, and W. J. Wadsworth, Opt. Express **18**, 16193 (2010).
[14] Y. Chen, W. J. Wadsworth, and T. A. Birks, Opt. Lett. **38**, 3747 (2013).
[15] C. J. McKinstrie, and M. G. Raymer, Opt. Express **14**, 9600 (2006).
[16] Arismar Cerqueira S. Jr, J. M. Chavez Boggio, A. A. Rieznik, H. E. Hernandez-Figueroa, H. L. Fragnito, and J. C. Knight, Opt. Express **16**, 2816 (2008).
[17] K. L. Vodopyanov, E. Sorokin, I. T. Sorokina, and P. G. Schunemann, Opt. Lett. **36**, 2275 (2011).
[18] H. Sayinc, M. Wysmolek, J. M. Chavez Boggio, R. Haynes, M. M. Roth, U. Morgner, J. Neumann, and D. Kracht, Appl. Phys. B **110**, 299 (2013).
[19] C.Y. Wang, T. Herr, P. Del'Haye, A. Schliesser, J. Hofer, R. Holzwarth, T.W. Hänsch, N. Picqué, and T. J. Kippenberg, Nat. Commun. **4**, 1345-1 (2013).
[20] Y. Li, J. Hou, Z. F. Jiang, L. J. Huang, and J. Y. Leng, Appl. Opt. **53**, 1583 (2014).
[21] T. L. Cheng, L. Zhang, X. J. Xue, D. H. Deng, T. Suzuki, and Y. Ohishi, Opt. Express **23**, 4125 (2015).
[22] J. H. Yuan, X. Z. Sang, Q. Wu, G. Y. Zhou, C. X. Yu, K. R. Wang, B. B. Yan, Y. Han, G. Farrell, and L. T. Hou, Opt. Lett. **38**, 5288 (2013).
[23] M. H. Frosz, P. Falk, and O. Bang, Opt. Express **13**, 6181 (2005).
[24] S. Murugkar, C. Brideau, A. Ridsdale, M. Naji, P. K. Stys, and H. Anis, Opt. Express **15**, 14028 (2007).
[25] J. H. Yuan, X. Z. Sang, C. X. Yu, Y. Han, G. Y. Zhou, S. G. Li, and L. T. Hou, J. Lightw. Technol. **29**, 2920 (2011).
[26] S. Lefrancois, D. Fu, G. R. Holtom, L. J. Kong, W. J. Wadsworth, P. Schneider, R. Herda, A. Zach, X. S. Xie, and F. W. Wise, Opt. Lett. **37**, 1652 (2012).
[27] M. L. Hu, C.Y. Wang, Y. J. Song, Y. F. Li, and L. Chai, Opt. Express **14**, 1189 (2006).

References

[1] P. St. J. Russell, "Photonic Crystal Fibers," J. Lightw. Technol., vol.24, pp.4729-4749, 2006.

[2] J. M. Dudley, G. Genty, and S. Coen, "Supercontinuum generation in photonic crystal fiber," Rev. Mod. Phys., vol.78, pp.1135-1184, 2006.

[3] A. A. Cumberland, J. C. Travers, S. V. Popov, and J. R. Taylor, "Toward visible cw-pumped supercontinua," Opt. Lett., vol.33, pp.2122-2124, 2008.

[4] J. M. Dudley, and J. R. Taylor, "Ten years of nonlinear optics in photonic crystal fibre," Nat. Photon., vol.3, pp.85-90, 2009.

[5] S. P. Stark, J. C. Travers, and P. St. J. Russell, "Extreme supercontinuum generation to the deep UV," Opt. Lett., vol.37, pp.770-772, 2012.

[6] I. Cristiani, R. Tediosi, L. Tartara, and V. Degiorgio, "Dispersive wave generation by solitons in microstructured optical fibers," Opt. Express, vol.12, pp.124-135, 2004.

[7] H. H. Tu, and S. A. Boppart, "Optical frequency up-conversion by supercontinuum-free widely-tunable fiber-optic Cherenkov radiation," Opt. Express, vol. 17, pp. 9858-9872, 2009.

[8] G. Q. Chang, L. J. Chen, and F. X. Kärtner, "Highly efficient Cherenkov radiation in photonic crystal fibers for broadband visible wavelength generation," Opt. Lett., vol. 35, pp. 2361-2363, 2010.

[9] G. P. Agrawal, Applications of Nonlinear Fiber Optics (Academic, 2008).

[10] N.Y. Joly, J. Nold, W. Chang, P. Hölzer, A. Nazarkin, G. K. L. Wong, F. Biancalana, and P. St. J. Russell, "Bright Spatially Coherent Wavelength-Tunable Deep-UV Laser Source Using an Ar-Filled Photonic Crystal Fiber," Phys. Rev. Lett., vol. 106, pp. 203901-1-4, 2011.

[11] S. Asimakis, P. Petropoulos, F. Poletti, J. Y. Y. Leong, R. C. Moore, K. E. Frampton, X. Feng, W. H. Loh, and D. J. Richardson, "Towards efficient and broadband four-wave-mixing using short-length dispersion tailored lead silicate holey fibers," Opt. Express, vol. 15, pp. 596-601, 2007.

[12] D. Nodop, C. Jauregui, D. Schimpf, J. Limpert, and A. Tünnermann, "Efficient high-power generation of visible and mid-infrared light by degenerate four-wave-mixing in a large-mode-area photonic-crystal fiber," Opt. Lett., vol.34, pp.3499-3502, 2009.

[13] L. Lavoute, J. C. Knight, P. Dupriez, and W. J. Wadsworth, "High power red and near-IR generation using four wave mixing in all integrated fibre laser Systems," Opt. Express, vol.18, pp.16193-16205, 2010.

[14] Y. Chen, W. J. Wadsworth, and T. A. Birks, "Ultraviolet four-wave mixing in the LP_{02} fiber mode," Opt. Lett., vol. 38, pp. 3747-3750, 2013.

[15] C. J. McKinstrie, and M. G. Raymer, "Four-wave-mixing cascades near the zero-dispersion frequency," Opt. Express, vol. 14, pp. 9600-9610, 2006.

[16] Arismar Cerqueira S. Jr, J. M. Chavez Boggio, A. A. Rieznik, H. E. Hernandez-Figueroa, H. L. Fragnito, and J. C. Knight, "Highly efficient generation of broadband cascaded four-wave mixing products," Opt. Express, vol. 16, pp. 2816-2828, 2008.

[17] K. L. Vodopyanov, E. Sorokin, I. T. Sorokina, and P. G. Schunemann, "Mid-IR frequency comb source spanning 4.4-5.4 µm based on subharmonic GaAs optical parametric oscillator," Opt. Lett., vol. 36, pp. 2275-2277, 2011.

[18] H. Sayinc, M. Wysmolek, J. M. Chavez Boggio, R. Haynes, M. M. Roth, U. Morgner, J. Neumann, and D. Kracht, "Broadband-cascaded four-wave mixing in a photonic crystal fiber around 1 µm," Appl. Phys. B, vol. 110, pp. 299-302, 2013.

[19] C.Y. Wang, T. Herr, P. Del'Haye, A. Schliesser, J. Hofer, R. Holzwarth, T.W. Hänsch, N. Picqué, and T. J. Kippenberg, "Mid-infrared optical frequency combs at 2.5 µm based on crystalline microresonators," Nat. Commun., vol. 4, pp. 1345-1-7, 2013.

[20] Y. Li, J. Hou, Z. F. Jiang, L. J. Huang, and J. Y. Leng, "Cascaded four-wave mixing seeded by two continuous wave signals," Appl. Opt., vol. 53, pp. 1583-1590, 2014.

[21] T. L. Cheng, L. Zhang, X. J. Xue, D. H. Deng, T. Suzuki, and Y. Ohishi, "Broadband cascaded four-wave mixing and supercontinuum generation in a tellurite microstructured optical fiber pumped at 2 µm," Opt. Express, vol. 23, pp. 4125-4134, 2015.

[22] J. H. Yuan, X. Z. Sang, Q. Wu, G. Y. Zhou, C. X. Yu, K. R. Wang, B. B. Yan, Y. Han, G. Farrell, and L. T. Hou, "Efficient and broadband Stokes wave generation by degenerate four-wave mixing at the mid-infrared wavelength in a silica photonic crystal fiber," Opt. Lett., vol. 38, pp. 5288-5291, 2013.

[23] M. H. Frosz, P. Falk, and O. Bang, "The role of the second zero-dispersion wavelength in generation of supercontinua and bright-bright soliton-pairs across the zero-dispersion wavelength," Opt. Express, vol.13, pp.6181-6192, 2005.

[24] S. Murugkar, C. Brideau, A. Ridsdale, M. Naji, P. K. Stys, and H. Anis, "Coherent anti-Stokes Raman scattering microscopy using photonic crystal fiber with two closely lying zero dispersion wavelengths," Opt. Express, vol.15, pp.14028-14037, 2007.

[25] J. H. Yuan, X. Z. Sang, C. X. Yu, C. Y. Han, G. Y. Zhou, S. G. Li, and L. T. Hou, "Highly efficient anti-Stokes signal conversion by pumping in the normal and anomalous dispersion regions in the fundamental mode of photonic crystal fiber," J. Lightw. Technol., vol.29, pp.2920-2926, 2011.

[26] S. Lefrancois, D. Fu, G. R. Holtom, L. J. Kong, W. J. Wadsworth, P. Schneider, R. Herda, A. Zach, X. S. Xie, and F. W. Wise, "Fiber four-wave mixing source for coherent anti-Stokes Raman scattering microscopy," Opt. Lett., vol.37, pp.1652-1654, 2012.

[27] M. L. Hu, C.Y. Wang, Y. J. Song, Y. F. Li, and L. Chai, "Mode-selective mapping and control of vectorial nonlinear-optical processes in multimode photonic-crystal fibers," Opt. Express, vol.14, pp.1189-1198, 2006.